https://doi.org/10.5194/acp-2020-1244
Preprint. Discussion started: 16 December 2020


Atmospheric Chemistry and Physics Discussions

# Increase of secondary organic aerosol over four years in an urban environment

Marta Via[1,2], María Cruz Minguillón[1], Cristina Reche[1], Xavier Querol[1], Andrés Alastuey[1]

[1]Institute of Environmental Assessment and Water Research (IDAEA-CSIC), Barcelona, 08034, Spain

[2]Department of Applied Physics, University of Barcelona, Barcelona, 08028, Spain

*Correspondence to:* M. Via (marta.via@idaea.csic), M. C. Minguillón (mariacruz.minguillon@idaea.csic.es)

**Abstract**. The evolution of fine aerosol ($PM_1$) species as well as the contribution of potential sources to the total organic aerosol (OA) at an urban background site (Palau Reial, PR, 80 m a.s.l) in the western Mediterranean basin (WMB) was investigated. For this purpose, an aerosol chemical speciation monitor (ACSM) was deployed to acquire real-time measurements for two one-year periods: May 2014 - May 2015 (period A) and Sep 2017 - Oct 2018 (period B). Total $PM_1$ concentrations showed a slight decrease (from 10.1 to 9.6 $\mu g \cdot m^{-3}$ from A to B), although the relative contribution of both inorganic and organic compounds varied significantly.

Regarding inorganic compounds, $SO_4^{2-}$, black carbon and $NH_4^+$ showed a significant decrease from period A to B, whilst $NO_3^-$ concentration was found higher in B. Source apportionment revealed OA was 46% and 70% of secondary origin (SOA) in periods A and B, respectively. Two oxygenated secondary sources (OOA) were differentiated by their oxidation status (i.e. aging): less-oxidized (LO-OOA) and more-oxidized (MO-OOA). Disregarding winter periods, where LO-OOA production is not favoured, LO-OOA transformation into MO-OOA was found more effective in period B. The highest MO-OOA-to-LO-OOA ratio (1.5) was found in September-October 2018, implying an accumulation effect after the high temperature and solar radiation conditions in the summer season. In addition, SOA was found sensitive to a $NO_x$-polluted ambient and to other pollutants, especially to ozone, which could be enhancing its production specially during afternoon hours. The anthropogenic primary OA sources identified, cooking-like OA (COA), hydrocarbon-like OA (HOA), and biomass burning OA (BBOA), decreased from period A to B in both absolute concentrations and relative contribution (as a whole, 44% and 40%, respectively). However, their concentrations and proportion to OA grow rapidly during highly-polluted episodes.

The influence of certain atmospheric episodes on OA sources was also assessed. Both SOA factors seem linked with long and medium-range circulations, especially those coming from inland Europe and the Mediterranean (triggering mainly MO-OOA) and summer breeze-driven regional circulation (triggering mainly LO-OOA). In contrast, POA pollution is enhanced either during air-cleaning episodes or stagnation anticyclonic events.

## 1. Introduction

Atmospheric particulate matter (PM) is regarded by the World Health Organization as one of the most harmful air pollutants to human health (WHO, 2016, 2018). Fine particles ($PM_1$, those with aerodynamic diameter <1 µm) have a significant impact on human health (Trippetta et al., 2016; Yang et al., 2019, 2018), climate (Shrivastava et al., 2017), and visibility (Shi et al., 2014). Organic Aerosol (OA) is the main constituent of fine aerosol in the atmosphere (Zhang et al., 2007) and it can be classified regarding its origin as primary OA (POA), consisting of directly emitted solid or liquid OA; or secondary OA (SOA), resulting from chemical transformation of pre-existing particles, nucleation or gas-to-particle condensation.

https://doi.org/10.5194/acp-2020-1244
Preprint. Discussion started: 16 December 2020


Atmospheric Chemistry and Physics Discussions

The complex atmospheric dynamics of the Western Mediterranean Basin (WMB) have been described in Millán, 2014; Millán et al., 1997. The emissions of the densely populated, harbor-close, traffic-concurred and industrialized areas coupled to the breeze-driven regimes, complex topography and anticyclonic stagnation meteorological episodes prompt complex phenomena of transport and transformation. Previous non-refractory $PM_1$ (NR-$PM_1$) chemical characterization and OA source apportionment at urban background sites has been performed in Europe (e.g. Canonaco et al., (2015); El Haddad et al. (2013); Zhang et al.(2019a)) improving the comprehension of the origin of the fine aerosol and OA sources contribution. Nevertheless, contributions to OA are still not fully understood due to large variability of their fingerprints, response to atmospheric dynamics and transport and evolution processes dependent on site-specific meteorological characteristics and precursors provision.

The focus of the present study is on the sources contributing to the fine OA in an urban background site of the WMB and their evolution along a 4-year period. To this end, a Quadrupole Aerosol Chemical Speciation Monitor (Q-ACSM) was deployed to comprehend site-specific nature and cyclicality of OA contributors, as accurate source characterization knowledge is necessary to design mitigating strategies of the effects of specific pollutants.

## 2. Methodology

### 2.1 Sampling site and period

The urban background site Palau Reial (PR; 41° 23′ 15″ N; 02° 07′ 05″ E; 80 m a.s.l.) is located in a residential area at the NW of Barcelona and at 200 m distance from one of the most concurred avenues of the city (>60.000 vehicles per working day in 2014-2018) (City council of Barcelona, 2019). Traffic emissions are the main contributors to $PM_{2.5}$, although other contributing sources such as industry, dust or shipping have been reported (Amato et al., 2016). More recent studies focusing on $PM_1$ and including organic speciation, also present cooking-like and biomass burning OA and diverse secondary aerosol sources (Brines et al., 2019; Minguillón et al., 2016). The atmospheric dynamics of the area are dominated by breeze regimes, consisting in a nocturnal NW wind component, a diurnal breeze development turning from SE to SW direction, and highest wind speeds around noon (Pérez et al., 2004).

Two intensive monitoring campaigns were carried out during May 2014 to May 2015 and September 2017 to October 2018 periods, which will be called hereinafter as period A and period B, respectively. Data availability for each measurement type is shown in Fig. S1. From now on, averages and data of any variable or parameter will correspond to the periods when ACSM data is available.

### 2.2 ACSM settings, calibrations and data processing

A Q-ACSM (Aerodyne Research Inc.) was deployed at PR to measure NR-$PM_1$, distinguishing OA, $SO_4^{2-}$, $NO_3^-$, $NH_4^+$ and $Cl^-$ with a 30-minute resolution. The ACSM was connected to a general inlet with a 2.5 µm cut off using a flow rate of 3 $L \cdot min^{-1}$, conducted through a nafion dryer maintaining the incoming RH below 40%. The instrument samples ambient air at 0.1 $L \cdot min^{-1}$ through a critical orifice (100 µm in diameter) towards an aerodynamic lens which transmits particles between 75 and 650 nm (Liu et al., 2007). Particles are then flash-vaporized at 600°C in high vacuum conditions and ionized by hard-electron impact (70 MeV), and resulting fragments are analysed by a quadrupole mass spectrometer (Ng et al., 2011). The instrument is equipped with a filter-valve system, hence concentrations reported are the result of subtraction of particle-free to particle-laden signal. The fragmentation table (Allan et al., 2004), the ion transmission correction and Response Factor (RF), are used to convert the signal spectra into organic or inorganic species concentrations. Ionization Efficiency (IE) and Relative Ion Efficiency (RIE) calibrations were conducted using 300-nm monodispersed $NH_4NO_3$ and $(NH_4)_2SO_4$ particles (Ng et al., 2011).

https://doi.org/10.5194/acp-2020-1244
Preprint. Discussion started: 16 December 2020


Atmospheric Chemistry and Physics Discussions

Final values for IE and RIEs for $NH_4^+$ and $SO_4^{2-}$ respectively were $2.38 \cdot 10^{-11}$, 5.27, and 0.71 for period A; and $5.10 \cdot 10^{-11}$, 5.16, and 0.77 for period B.

The ACSM was operated with 24 scans per measurement (alternating sample/filter scan) with a scan speed of 200 ms·amu$^{-1}$, resulting in a 30-minute time resolution. Data acquisition software (versions 1.4.4.5, 1.5.2.1 and 1.6.0.0 depending on the period) and analysis software (version 1.6.1.1) implemented in Igor Pro (WaveMetrics, Inc.) were provided by Aerodyne Research Inc. Data were corrected to account for flow rate changes and for response decay by using the $N_2$ signal. The composition-dependent collection efficiency (CE) (Middlebrook et al., 2012) corrections were applied.

### 2.3 Additional measurements and instrumentation

Black Carbon (BC) concentrations were measured by a Multi-Angle Absorption Photometer (MAAP, Thermofisher 5012) with 1-minute time resolution. $PM_1$ concentrations were measured by: i) gravimetric method resulting from high volume samplers DIGITEL (DH-80); and ii) Optical Particle Counter (OPC, GRIMM 180, 10-minutal time resolution, corrected with gravimetric results). Particle number size distribution was measured by a Scanning Mobility Particle Sizer (SMPS, TSI 3936, 5-minutal time resolution, size-resolved particle number ranging 12-470 nm) and converted to mass concentrations based on composition-dependent aerosol density (DeCarlo et al., 2004). $SO_4^{2-}$, $NO_3^-$, $NH_4^+$ concentrations were determined in offline $PM_1$ samples by ICP-AES, chromatography and selective electrode methods. Organic Carbon (OC) concentrations were determined in offline $PM_1$ samples by thermal-optical methods. Procedures of filter samples analysis are detailed in Supplementary Section 1.

Real time gaseous pollutants measurements, NO, $NO_2$ (SIR S-5012), CO (Ecothec EC 9830), $O_3$ (SIR S-5014) and $SO_2$ (Thermo Scientific Model 43C), operated by the Department of Environment of the Autonomous Government of Catalonia, were available at a 1-minute resolution. Meteorological variables were provided by the Department of Meteorology of the University of Barcelona. In all data analysis, time will always be UTC based, unless otherwise specified.

Standardized protocols of quality control (COST Action CA16109 COLOSSAL Chemical On-Line cOmposition and Source Apportionment of fine aerosoL, 2019) were carried out in both periods. The sum of all NR-$PM_1$ species (OA + $SO_4^{2-}$ + $NO_3^-$ + $NH_4^+$ + $Cl^-$) and BC was compared with co-located $PM_1$ measurements. This analysis assumes that the $PM_1$ contribution of the mineral and sea salt tail from the coarse PM or the trace elements are negligible. Also, species concentrations obtained by Q-ACSM were compared with the same components from off-line $PM_1$ determination except for ACSM OA, which was compared with organic carbon (OC).

### 2.4 Source apportionment of OA

Source apportionment of the organic mass fraction was conducted applying the Positive Matrix Factorization (PMF) method (Paatero and Tapper, 1994), using the multilinear engine (ME-2) (Paatero, 1999), to OA mass spectra. It ranged from 12 to 120 Th and excluded higher m/z ions which accounted for minor fraction of total signal (<3% on average), presented low S/N ratio and were interfered by the naphthalene signal. The PMF model decomposes the bulk OA matrix by iterating

$$X = G \cdot F + E = \sum_{k=1}^{P} g_{i,k} f_{p,j} + e_{i,j} \quad (1)$$

where $X$ is the $m \cdot n$ measured OA matrix, $m$ is the number of rows of $X$, which consist of the number of time steps, and $n$ is its number of columns, which account for the number of $m/z$ from 12 to 120. $G$ is the matrix that denotes the contributions of a factor $p$ at a time step $i$ and F represents the contribution of ion $j$ to factor $p$ mass spectrum. The matrix $E$ is the residual matrix containing the unexplained information from $X$. The model consists of the iterative minimization of the error matrix by least-squares algorithm, where

https://doi.org/10.5194/acp-2020-1244
Preprint. Discussion started: 16 December 2020


Atmospheric Chemistry and Physics Discussions

$$Q = \sum_{i=1}^{n}\sum_{j=1}^{m}\left(\frac{e_{ij}}{\sigma_{ij}}\right)^2 \quad (2)$$

is the optimization variable. In order to avoid to conduct this function to not a global but a local minimum the whole *n·m* space should be covered, and to this end rotational tools are vital to converge to mathematically coherent solutions.

PMF allows to introduce a-priori information to guide the model, e.g. by using the *a-value* approach. Both factor profiles and time series can be restricted to resemble to introduced reference ones, named anchor profiles or anchor series. By means of a parameter *a*, the percentage of freedom of a given factor respect to their constraint can be varied.

Each dataset was separated in four periods: April-May, June-August, September-October and November-March. Modifications from standard seasons were based on the monthly-averaged concentration of BBOA markers (f60, f73), only revealing a potential BBOA source from November to March (Fig. 4), and meteorological variables.

The OA source apportionment was carried out following the methodology described by Crippa et al. (2013) and COLOSSAL guidelines (work in progress), using the SoFi (Source Finder) toolkit version 6.8k developed by Datalystica Ltd. Unconstrained PMF was performed with 3 to 8 factors runs and posteriorly, PMF with constraints was run with 3 to 5 or to 6 factors depending on the season. Differences between solutions of different number of factors for each season are shown in Table S1, Fig. S 2 and chosen seasonal profiles in Fig. S3. The constraints applied through ME2 for HOA and COA sources used the anchor profile of (Crippa et al., 2013), as the solutions anchored with them correlated better with the external tracers than those anchored with Mohr et al., 2012 (Table S2). The profile anchor used for BBOA was from Ng et al., 2010. In all cases, they all were subject to a sensitive analysis with a-values ranging 0-0.5 and steps of 0.1 to choose the best a-value combination for these three factors. Optimization of the number of factors and a-value combinations implied considering (Table S1): i) variation of the ratio between $Q/Q_{exp}$ ($Q_{exp} = m \cdot n - p \cdot (m + n)$), which should present a steady descent from *p* to *p+1*, *p+2* factors, being *p* the chosen number of factors; ii) correlation of time series of OA factors with tracers; iii) scaled residuals of profiles and time series; iv) agreement between apportioned and measured OA concentrations; v) gathered knowledge of site-specific atmosphere and potential sources.

The resulting factors were interpreted as cooking-like OA (COA), hydrocarbon-like OA (HOA), biomass burning OA (BBOA) (only identified in cold periods) and two oxidized OA (OOA) factors named less-oxygenated OOA (LO-OOA) and more-oxygenated OOA (MO-OOA).

### 2.5 Classification of atmospheric episodes.

Classification of atmospheric episodes was performed with the HYSPLIT model (Stein et al., 2015). Air mass back-trajectories for 120 h at three heights (750, 1500 and 2500 m a.s.l) were computed, with vertical flux modelling, for each day of measurements and interpreted to be classified regarding its predominant transport provenance into Atlantic North (AN), Winter Anticyclonic (WA) (from October to March), Europe (EU), Mediterranean (MED), North African (NAF) and Summer Regional (SREG, from April to September), characteristics of which are discussed in previous works (Pey et al., 2010; Ripoll et al., 2014, 2015).

## 3. Results

### 3.1 Comparison of ACSM data with co-located measurements.

Comparison of ACSM output with co-located measurements can be found in Table S3. OPC shows the best agreement with ACSM (NR-$PM_1$+BC vs. OPC $PM_1$), with Squared Pearson correlation coefficients $R^2$=0.71 and $R^2$=0.76 and slopes of the

https://doi.org/10.5194/acp-2020-1244
Preprint. Discussion started: 16 December 2020


Atmospheric Chemistry and Physics Discussions

orthogonal distance fit 0.989 ± 0.007 and 1.285 ± 0.006 for periods A and B, respectively. The slopes over 1 when comparing ACSM with other instruments can be partially attributed to differences in the particle size range measured. Moreover, overestimation of primary OA sources by ACSM by a factor of 1.2 to 1.5 has also been reported (Reyes-Villegas et al., 2018; Xu et al., 2018) as a consequence of source-unspecific OA RIE application, leading in turn to $PM_1$ overestimation by ACSM.

Very good agreement is shown between off-line analysis of $SO_4^{2-}$, $NO_3^-$ and $NH_4^+$ ($R^2$>0.85) and also between OA and organic carbon (OC) ($R^2$=0.73 in A and $R^2$=0.86 in B). The anion $Cl^-$ is not considered due to the very low concentrations and potential determination problems (Tobler et al., 2020). OA-to-OC ratio is estimated from the slope in the scatterplot between these two variables, resulting in a value of 2.69 and 2.96 in periods A and B, respectively, a 68% and 85% higher than the 1.6 value found in Barcelona (Minguillón et al., 2011), calculated as in (Aiken et al., 2008). This OA-to-OC ratios would point, similarly to the previous findings at Montsec (Ripoll et al., 2015) and Montseny (Minguillón et al., 2015), to the aforementioned unspecific-source OA RIE overestimation in ACSM and the artifact evaporation of semi-volatile compounds of OC in filters.

### 3.2 Submicron aerosol composition

Data overview for periods A and B is shown in Table S4. Time series of NR-$PM_1$ species, co-located gases and meteorological parameters are shown in Fig. S 4, Fig. S 5 and Fig. S 6, respectively.

Average $PM_1$ concentrations (± standard deviation) resulting from the sum of NR-$PM_1$ components and BC are 10.1 ± 6.7 $\mu g \cdot m^{-3}$ during campaign A and 9.6 ± 6.6 $\mu g \cdot m^{-3}$ during campaign B (reduction of a 5% from A to B). A decrease of a 5%, 21%, 9% and 18% is shown for of OA, $SO_4^{2-}$, $NH_4^+$ and BC, respectively, although $NO_3^-$ and $Cl^-$ increased an 8% and a 20% from period A to B.

In both periods, OA was the largest contributor to $PM_1$, accounting for (average ± standard deviation) 43%±10% and 44%±17% of the total average mass (ACSM NR-$PM_1$ species + BC), followed by $SO_4^{2-}$ (19%±11% and 18%±10%), BC (17%±9% and 13%±10%), $NO_3^-$ (10%±8% and 13%±10%), $NH4^+$ (11%±8% and 11%±6%), and $Cl^-$ (0.4%±0.8% and 0.8%± 0.9%), respectively, for periods A and B.

#### 3.2.1 Seasonal variation

Seasonally averaged mean $PM_1$ species concentrations are displayed in Fig. 1 for both periods, and time series in Fig. S 4. In period A, $PM_1$ highest concentrations occur in Sep-Oct and followed by short by concentrations in Apr-May, being the lowest records in summer. Contrastingly, in period B, submicron aerosol is maximum in summer and minimum in winter. The differences in meteorological situations, occurrence frequency of atmospheric episodes and data availability might be a direct cause of these mismatches of seasonal trends. The frequency of occurrence of episodes per month differs significantly from period A to period B (Fig. S7), leading to different $PM_1$ concentrations for the same months of different periods. In June, July and August, for instance, the ratio of occurrence of SREG/AN is lower in period A than in period B, which is coherent with lower $PM_1$ concentrations recorded in July A with respect to July B.

OA seasonal trend behaves similarly as bulk NR-$PM_1$ due to same causes, but also photochemical enhancement in warm months due to higher sun irradiation, except for summer 2014. $SO_4^{2-}$ concentrations are in both cases higher during warmer than colder months, opposite to the $NO_3^-$ concentrations trend (except for September-October 2014) as has been widely reported in previous studies (Minguillón et al., 2015; Pey et al., 2009; Ripoll et al., 2015). In period A, higher $NH_4^+$ concentrations happen during winter months whilst they are seasonally-stable through period B. BC shows the lowest concentrations in summer months in both periods, although this decrement is more pronounced in period A.

### 3.3 OA source apportionment

https://doi.org/10.5194/acp-2020-1244
Preprint. Discussion started: 16 December 2020


Atmospheric Chemistry and Physics Discussions

The chosen solution contained 5 factors, interpreted as COA, HOA, BBOA, considered primary OA (POA), and two secondary oxidized OA factors, LO-OOA and MO-OOA. This is consistent with previous campaigns performed in Barcelona using both ACSM (Minguillón et al., 2016) and AMS (Mohr et al., 2012, 2015) in which same OA sources were identified. Just for the cold season in period A, a single OOA factor was extracted. Supporting the solutions chosen, mean scaled residuals (Fig. S 7) are sharply centered to zero in both cases although histogram A shows higher spread and skewness, meaning worse match between OA measured and the sum of OA factors concentrations.

COA accounts for a 18% and 14% (period A and B, respectively) of OA (Fig. 2). COA profiles (Fig. 3) reflect the expected pattern of signals related to the oxygenation of fatty acids due to cooking activities (*m/z* 29, 55, 41, 69) (He et al., 2010). Correlation between COA and HOA is not negligible, as profiles show a Pearson coefficient of $R^2 \geq 0.71$ (Table S2). However, the time series of these factors varies independently ($R^2 > 0.20$ except for Sep-Oct 2014), which allows for some confidence in their separation. The time series of COA does not show a significant seasonal trend (Fig. 4, Fig. 5). Correlation with *m/z* 55, the main COA marker, is 0.58 and 0.71 in A and B, respectively. Diel cycles present peaks at around 1 PM and 9 PM, coinciding with lunch and dinner hours and another at 9 AM probably entangled with the traffic peak at same hour (Fig. 6, Fig. S 8). Figure 5 also reveals a much higher dinner peak than the lunch peak along almost all seasons, probably related to a much thinner planet boundary layer (PBL) at 9 PM than at 1 PM.

HOA consists mainly of ions stemming from diesel exhaust from recondensed engine lubricating oil compounds (Canagaratna et al., 2010; Chirico et al., 2010). Average contributions in periods A and B are, respectively, 20% and 12% (
Figure **2**). HOA concentrations follow a decreasing seasonal pattern towards summer months (Fig. 4, Fig. 5) which could be associated to lower traffic intensity in August, the thicker boundary layer, the maximum recirculation induced by the highest speeds of sea-breeze and a likely faster oxidation of the primary HOA due to higher temperatures. Diel patterns (Fig. 6, Fig. S8) reproduce two traffic-associated peaks at 7 AM and 8 PM in both periods, reduced during summer months, resembling traffic cycles (Fig. S9). Correlations with BC are $R^2$=0.63, 0.68 and with $NO_x$ are $R^2$=0.44, 0.65, in periods A and B, respectively, and remarkably weaker in summer periods ($R^2_{min}$=0.29, 0.51, respectively) accompanied with a decrease in the HOA-to-BC ratio.

BBOA mass spectra is alike in both cold periods (Fig. 3) characterized by ions at *m/z* 29, 43, 60 and 73, fragments of anhydrosugars, such as levoglucosan, products of cellulose pyrolysis combustion reactions (Alfarra et al., 2007). BBOA is only abiding by the coldest period, from November to March (Fig. 4) and accounting for 14% and 12% of total OA in A and B, respectively. Diel cycles present the same trend in both periods (Fig. S8), staying flat throughout the day and ascending from 7 PM to 0 AM, pointing to a relation to nocturnal domestic heating or breeze-driven transported pollutants from forest or agricultural fires (Reche et al., 2012) and enhanced by a narrower boundary layer. Correlations with ions *m/z* 60 and *m/z* 73 are better in period B ($R^2$=0.91 and 0.61, respectively) than in period A ($R^2$=0.60 and 0.55, respectively) (Table S2).

Secondary organic aerosol (SOA) factors are resolved freely by the model. They are known to be determined mostly by *m/z* 43 and *m/z* 44, which indicate the degree of oxidation (Canagaratna et al., 2015). The fractions of *m/z* 44 and *m/z* 43 over apportioned OA (*f44, f43*) scattered per seasons are shown in Fig. S 10. In cold months dots are less concentrated and they withdraw from the expected triangle proposed by (Ng et al., 2010) due to a worst definition of SOA factors, besides some might be untrustworthy because they are close to the OA detection limit. Atmosphere is inferred to be more oxidized in period B, especially in summer months as clouds of points present lower *f43* and higher *f44* than in A. This is reflected in the OOA factors discussed below.

https://doi.org/10.5194/acp-2020-1244
Preprint. Discussion started: 16 December 2020


Atmospheric Chemistry and Physics Discussions

LO-OOA mass spectra differs significantly from period A to B. The *m/z* 43-to-*m/z* 44 ratio is 0.37 in period A and 1.05 in period B (Fig. 3), indicating a LO-OOA profile with a higher oxidation degree in period A. Contribution of LO-OOA to apportioned OA increased from period A to B although the period average is not directly comparable, as period A lacks this factor in the cold period, hence considered as zero and leading to lower LO-OOA concentrations (Fig. 2). Considering only the three seasons excluding the Nov-Mar period, LO-OOA shows a slight decrease from period A to B (1.6 $\mu g \cdot m^{-3}$ to 1.5 $\mu g \cdot m^{-3}$). Seasonally, in all cases except for the already discussed summer 2014, the amount of this source decreased from period A to B. In both cases, LO-OOA concentrations rise towards warmer months, which suggests SOA formation pathways might be linked to photochemical oxidation and breeze regimes. This can also be inferred by the diel patterns of LO-OOA (Fig. S 8), which are flat except for a valley of around a factor of -30% from 2 to 8 PM, when temperature and irradiation reach their maximums, but also related to PBL widening and maximum sea breeze speeds at the time. The rise in LO-OOA at night could be also explained by nighttime SOA formation via $NO_3$ radical (result of anthropogenic $NO_x$ reactions) oxidation of VOCs, but especially due to the land breeze prevailing during the night and transporting previously formed OA from inland areas to the coast. The valleys around 3PM of seasonal diel cycles do seem to be more profound in April-May and June-August and the peak-to-valley ratio more pronounced in period B (Fig. 6).

MO-OOA mass spectra are similar for periods A and B, even including the OOA profile from the cold subperiod in A. Excluding the Nov-March subperiod, MO-OOA shows an increase of a 90% (from 1.0 $\mu g \cdot m^{-3}$ to 1.9 $\mu g \cdot m^{-3}$ in A and B, respectively). The *m/z*43-to-*m/z*44 ratios are of 0.28 and 0.21, respectively, and hence, a less oxidized MO-OOA in period A (Fig. 3). MO-OOA apportions a 30% and a 42% of OA in periods A and B, respectively and this difference should be indeed widened as MO-OOA in subperiod Nov-Mar 2014-2015 is clearly overestimated (as all OOA is accounted as MO-OOA). Figure 5 supports the increase of magnitude from A to B in all seasons and highest seasonal concentrations in November-March 2014-2015 (due to a single OOA factor) followed by September-October 2014, September-October 2018 and June-August 2018. Thereof, origin of MO-OOA might be explainable from the photochemical transformation from LO-OOA oxidation, triggered amongst others by high temperatures. Diel cycles do not show any remarkable peaks or valleys (Fig. S 8).

Concentrations of the secondary factors as a function of temperature and $NO_x$ and CO concentrations for winter (DJF) and summer (JJA) are shown in Fig. S11. A tendency of higher concentrations of SOA towards higher temperatures and $NO_x$ concentrations in winter and summer can be observed. Temperature has been reported to enhance SOA photochemical pathways from VOCs; these graphs indicate, as pointed out in (Minguillón et al., 2016), that these reactions are also favored over a certain $NO_x$ concentration threshold. However, high concentrations of SOA are simultaneously high with high temperature and CO levels, inferring SOA might be enhanced not only by a highly $NO_x$-polluted ambient, but the ensemble of pollutants during severely-contaminated episodes.

Ozone has been reported to be an atmospheric oxidant inducing SOA production, whose period-averaged concentrations are substantially higher in period A than in B (Tables S4). Still, Figure S12 points out that ozone is more reactive in the period B, as the area of the difference between PR concentrations and those in the regional background site MSY (Montseny Natural Park, 720 m a.s.l, 40 km north–northeast of Barcelona and 25km from the Mediterranean coast) is higher during period B. This corresponds to the previously reported observation (Massagué et al., 2019) that ozone diel concentrations are flatter in MSY because mountain sites are less affected by NO titration, leading to high daily $O_3$ average concentrations. Therefore, the highest difference between MSY and PR, the more ozone has been reacting at PR. Enhanced reactivity of ozone in period B could be attributed to the reaction with higher VOCs concentrations resulting in the production of SOA. Also, contrasting $O_3$ and LO-OOA diel cycles, afternoon hours it can be seen how the LO-OOA increase coincides with the $O_3$ minimum.

https://doi.org/10.5194/acp-2020-1244
Preprint. Discussion started: 16 December 2020


Atmospheric Chemistry and Physics Discussions

Main contributors to high pollution episodes can be targeted monitoring the proportion of each factor to the total OA concentration as in Fig. 7 (Zhang et al., 2019b). In period A, concentrations of POA increase along with OA concentrations. However, in period B, with reduced POA concentrations respect to A, SOA represents the main pollutant even during OA growth, and more concretely, LO-OOA increases at expenses of MO-OOA. This points out that whilst POA was more responsible of high pollution episodes in A, this tendency was inverted over period B, as SOA is reasonably constant in B through OA growth except for the largest OA class. The highest episodes of OA in B are dominated by LO-OOA, taking the lead respect to MO-OOA as its formation temperature-driven generation pathway is faster than the ageing to a more oxidized form. Thus, the sudden increase of primary pollutants might provoke a fast enhancement of LO-OOA, whilst MO-OOA response is slower to these stimuli.

### 3.4 Spatial origin of OA.

Figure 8 shows wind rose plots and wind-direction-dependent concentrations of OA factors. The greatest frequency (up to 15%) of winds were associated with southwestern wind directions and highest wind speeds are related to the north-eastern directions. Frequency of types of episodes by moths, NR-$PM_1$ relative concentrations by episodes and absolute concentrations are shown in Fig. S 13.

Highest concentrations of COA are under northern and eastern winds under 4 and 8 m/s, respectively, indicative of advections from residential areas on the north and east of the site. HOA is the most local factor, presenting its highest values with stagnation regardless of the direction, and despite the proximity to one of the most concurred roads of Barcelona, hence showing that the HOA concentrations are driven by the general variation of the urban background and not by the direct emissions from this specific road. BBOA levels are high for low wind speeds (< 6m/s) mainly coming from western and northeastern directions, i.e. from residential areas nearby the site. Regional production seems to be the main cause of LO-OOA as well as northern and northwestern advections, transporting air masses inland. Eastern and north-eastern winds have been reported to recirculate pollutants from the outlying industrialized areas which are canalized through the Llobregat river basin. MO-OOA long-range transport is deduced from the plots, since highest concentrations are driven by stronger wind speeds from northeast in period A, and northwest, southwest and east in period B. Note that the main directions for both LO-OOA and MO-OOA in period B coincide, while the origin for LO-OOA and MO-OOA in period A seems to differ. This could be due to additional/missing source foci or changes in their advective pathways.

Regarding air masses, in Fig. 9, the proportion of OA of each source per episode is shown. Proportion of SOA is highest for SREG, coinciding with high temperatures, and coherent with the enhanced oxidation over time during these air mass recirculation episodes. High proportion is also recorded for EU and MED in period B. For the rest of episodes there is not a clear variation in terms of SOA contribution. Regarding absolute concentrations, the pattern is different for periods A and B (Fig. S9b). The highest concentrations are reached during WA episodes in period A, linked to stagnation conditions, and lowest during SREG, due to major occurrence in an aforementioned anomalously cold, wet summer (Servei Meteorològic de Catalunya, 2020a, 2020b). For period B, the highest concentrations correspond to MED and EU episodes, while the lowest were recorded during AN due to associated northern strong winds. Highest proportion of LO-OOA occurs for AW and SREG episodes, the first carrying pollutants which have crossed the whole Iberian Peninsula and the latter recirculating them along the breeze regime. MO-OOA is dominant in the highly polluted MED episodes, western advections and EU episodes, which provide long-range-driven pollutants from continental Europe.

## 4. Discussion

https://doi.org/10.5194/acp-2020-1244
Preprint. Discussion started: 16 December 2020


Atmospheric Chemistry and Physics Discussions

While bulk $PM_1$ decreased slightly from period A to B, with consistent decreases of all its main constituents except for $NO_3^-$, the average OA concentrations remain similar in both periods (4.2, 4.0 $\mu g \cdot m^{-3}$). Nevertheless, the relative contribution of the different OA sources varies significantly. The severe reduction of POA found from period A to B (-31%) is mainly driven by a significant decrement of HOA (-40%). The simultaneous reduction in BC and $NO_x$ concentrations of 18% and 4% point to an effect of traffic-restriction implemented policies. On the other hand, SOA concentrations increased from A to B both in absolute and relative terms, representing a 45% and 60% of total OA in periods A and B, respectively. The predominance of the SOA over total OA in period B remains also for the highly polluted episodes, where there is an increase of the relative POA contributions, but they still remain below 50% of total OA. Digging into SOA composition, it is more aged in period B, as shown by the increase of MO-OOA component at expenses of the LO-OOA reduction, becoming the main OA constituent in period B. This enhanced OA oxidation might be a result of the increment of the oxidization potential of the atmosphere, reported by recent studies in southern Europe (Saiz-Lopez et al., 2017), which could cause faster oxidization of fresh OA. This agrees with the increase of reactivity of ozone in the study area, as determined by the variations of urban and regional locations.

The temperature and solar radiation seem to enhance SOA concentrations, as shown by the pronounced seasonality, growing from cold to warm months (Fig. 5). The ratio LO-OOA-to-MO-OOA decreases strongly from period A to period B (mean average of 1.8 and 0.8), with lower values in autumn than summer for both A and B periods. This observation could be explained by an accumulation on MO-OOA after summer months due to progressive conversion of LO-OOA to MO-OOA under high temperature conditions and a prone oxidation of the OA in the atmosphere. This fact is supported by the increasing background from period A to B of f44 (and conversely, reduction of f43) (Fig. S 10), especially during summer months.

COA, HOA and BBOA are shown to be generated locally or short-range advected from residential areas and enhanced in proportion under stagnation WA episodes, i.e., when those emissions remain in the atmosphere and no advections carry them away, but also under and air-cleaning AN strong wind events, when air is pure and only local pollutants are present (formation of OOA is a slower pathway). Conversely, OOA factors are more likely to be transported by medium-range northern and eastern advections, although they can also be locally produced. Long-range transport episodes (EU and MED) and SREG episodes show the highest proportions of SOA. The maximum LO-OOA-to-MO-OOA ratio corresponds to SREG episodes, pointing to local SOA formation as the summer breeze recirculation might enhance fresh SOA. On the contrary, the lowest LO-OOA-to-MO-OOA ratio is recorded during EU and MED, indicative of aged SOA transport.

## 5. Conclusions

Characterization of non-refractory fine aerosol (NR-$PM_1$) in the urban background of Barcelona, including organic aerosol (OA) source apportionment, was performed regarding two nearly one-year periods between 2014 and 2018. Period-averaged $PM_1$ concentrations are 10.1 and 9.6 $\mu g \cdot m^{-3}$ respectively for the so-called periods A (May 2014 - May2015) and B (September 2017-October 2018). Strong correlation ($R^2$>0.71) between total mass concentration of ACSM species and BC and $PM_1$ retrieved by an optical counter, although slopes over 1 suggest an overestimation likely caused by the use of the default relative ionization efficiency for OA, which could be lower than the actual one.

The OA was the major component in both periods under study, accounting for a 43% and 44% of total $PM_1$. Five organic sources were identified by PMF: Cooking-like OA (COA), Hydro-Carbon-like OA (HOA), Biomass Burning OA (BBOA), Less-Oxidized Oxygenated OA (LO-OOA) and More-Oxidized Oxygenated OA (MO-OOA). BBOA was only present in the subperiod November-March and only one OOA factor was apportioned in the cold subperiod in 2014-2015. Secondary OA (SOA) proportion increased from the first period to the second, as well as absolute concentrations, while primary OA (POA)

https://doi.org/10.5194/acp-2020-1244
Preprint. Discussion started: 16 December 2020


Atmospheric Chemistry and Physics Discussions

concentrations were reduced. In turn, LO-OOA and MO-OOA have changed its relevance in OOA contributions, being the most oxidized the promoted one from 2014-2015 towards 2017-2018. This evidences a steady oxidation of OA components, more pronounced in warm periods and an increase in atmosphere oxidation conditions resulting in higher MO-OOA contribution. Solar radiation and temperature, from noon to around 5 PM, enhance the convection processes, increasing the thickness of the planetary boundary layer and consequently causing deep valleys in all factor diel cycles. Besides, photochemistry reactions have also been shown to encourage LO-OOA production and its conversion, in turn, to MO-OOA.

Seasonal variation of OA contributions was also affected by air masses origin. Northern flows and stagnation episodes induce primary pollution events, although high-SOA events are driven by long-range episodes, comprising Mediterranean and European advections (mainly MO-OOA), and regional breeze-driven recirculation (mainly LO-OOA).

Average contributions of the inorganic NR-$PM_1$ are 19% and 18% for $SO_4^{2-}$, 16% and 13% for black carbon (BC), 10% and 13% for $NO_3^-$, 11% and 11% for $NH_4^+$ and <1% for $Cl^-$ for periods A and B, respectively. Hence $SO_4^{2-}$ and BC concentrations decrease from A to B, while $NO_3^-$ ascends. Seasonal cycles maximize OA and $SO_4^{2-}$ in the warmer subperiod and $NO_3^-$ (high volatility in hot conditions) and BC in the coldest. $NO_x$ has also been reduced on average from A to B, as well as $O_3$ and $SO_2$. Nevertheless, $O_3$ has become more reactive on period B, therefore becoming a probable promoter of OA oxidation.

To the authors' knowledge, this is one of the first times NR-$PM_1$ chemical composition and OA sources have been studied with detail during a period long-enough to allow for conclusions on 4-years changes. The results obtained highlight the role of SOA as the main source of OA and its permanency even if POA is reduced. Furthermore, the remaining unexplained gaps about the oxidation of the urban-background atmosphere of Barcelona, possible pathways of production and transformation of SOA and interfering $O_3$ processes could be the objective of further investigations.

*Data availability.* All data used in this study can be accessed here: http://dx.doi.org/10.17632/xfv7z6jzcm.1

*Author's contributions.* Study was designed by MCM, AA and XQ. Measurements were carried out by MV, MCM and CR. Data analysis was done by MV and MCM. Data interpretation was done by MV, MCM and AA, with contributions and discussions with CR and XQ. MV wrote the manuscript with contributions from MCM. All the authors revised the manuscript and agreed with its final version.

*Competing interests.* The authors declare that they have no conflict of interest.

*Acknowledgements*. This work was supported by COST Action CA16109 COLOSSAL, the Generalitat de Catalunya (AGAUR 2017 SGR41), and the Spanish Ministry of Science and Innovation through CAIAC project (PID2019-108990RB-I00). Jordi Massagué is acknowledged for providing the $O_3$ data from Autonomous Governement of Catalonia.

**References**

Alfarra, M. R., Prevot, A. S. H., Szidat, S., Sandradewi, J., Weimer, S., Lanz, V. A., Schreiber, D., Mohr, M. and Baltensperger, U.: Identification of the mass spectral signature of organic aerosols from wood burning emissions, Environ. Sci. Technol., 41(16), 5770–5777, doi:10.1021/es062289b, 2007.

Amato, F., Alastuey, A., Karanasiou, A., Lucarelli, F., Nava, S., Calzolai, G., Severi, M., Becagli, S., Gianelle, V. L., Colombi,

https://doi.org/10.5194/acp-2020-1244
Preprint. Discussion started: 16 December 2020




C., Alves, C., Custódio, D., Nunes, T., Cerqueira, M., Pio, C., Eleftheriadis, K., Diapouli, E., Reche, C., Minguillón, M. C., Manousakas, M. I., Maggos, T., Vratolis, S., Harrison, R. M. and Querol, X.: AIRUSE-LIFE+: A harmonized PM speciation and source apportionment in five southern European cities, Atmos. Chem. Phys., 16(5), 3289–3309, doi:10.5194/acp-16-3289-2016, 2016.

Brines, M., Dall'Osto, M., Amato, F., Minguillón, M. C., Karanasiou, A., Grimalt, J. O., Alastuey, A., Querol, X. and van Drooge, B. L.: Source apportionment of urban PM1 in Barcelona during SAPUSS using organic and inorganic components, Environ. Sci. Pollut. Res., 26(31), 32114–32127, doi:10.1007/s11356-019-06199-3, 2019.

Canagaratna, M. R., Onasch, T. B., Wood, E. C., Herndon, S. C., Jayne, J. T., Cross, E. S., Miake-Lye, R. C., Kolb, C. E. and Worsnop, D. R.: Evolution of vehicle exhaust particles in the atmosphere, J. Air Waste Manag. Assoc., 60(10), 1192–1203, doi:10.3155/1047-3289.60.10.1192, 2010.

Canagaratna, M. R., Jimenez, J. L., Kroll, J. H., Chen, Q., Kessler, S. H., Massoli, P., Hildebrandt Ruiz, L., Fortner, E., Williams, L. R., Wilson, K. R., Surratt, J. D., Donahue, N. M., Jayne, J. T. and Worsnop, D. R.: Elemental ratio measurements of organic compounds using aerosol mass spectrometry: Characterization, improved calibration, and implications, Atmos. Chem. Phys., 15(1), 253–272, doi:10.5194/acp-15-253-2015, 2015.

Canonaco, F., Slowik, J. G., Baltensperger, U. and Prévôt, A. S. H.: Seasonal differences in oxygenated organic aerosol composition: Implications for emissions sources and factor analysis, Atmos. Chem. Phys., 15(12), 6993–7002, doi:10.5194/acp-15-6993-2015, 2015.

Chirico, R., Decarlo, P. F., Heringa, M. F., Tritscher, T., Richter, R., Prévôt, A. S. H., Dommen, J., Weingartner, E., Wehrle, G., Gysel, M., Laborde, M. and Baltensperger, U.: Impact of aftertreatment devices on primary emissions and secondary organic aerosol formation potential from in-use diesel vehicles: Results from smog chamber experiments, Atmos. Chem. Phys., 10(23), 11545–11563, doi:10.5194/acp-10-11545-2010, 2010.

City council of Barcelona, S. de M.: Volum de trànsit (Intensitat mitjana diària de vehicles en dia feiner) a les principals vies. 2014-2018, 2014-2018 [online] Available from: https://www.bcn.cat/estadistica/catala/dades/anuari/cap15/C1511010.htm (Accessed 13 May 2020), 2019.

COST Action CA16109 COLOSSAL Chemical On-Line cOmposition and Source Apportionment of fine aerosoL, W. G. 1: Guidelines for comparison of ACSM measurements with co-located external data, , Deliverabl(December 2019), 1–10, 2019.

Crippa, M., Decarlo, P. F., Slowik, J. G., Mohr, C., Heringa, M. F., Chirico, R., Poulain, L., Freutel, F., Sciare, J., Cozic, J., Di Marco, C. F., Elsasser, M., Nicolas, J. B., Marchand, N., Abidi, E., Wiedensohler, A., Drewnick, F., Schneider, J., Borrmann, S., Nemitz, E., Zimmermann, R., Jaffrezo, J. L., Prévôt, A. S. H. and Baltensperger, U.: Wintertime aerosol chemical composition and source apportionment of the organic fraction in the metropolitan area of Paris, Atmos. Chem. Phys., 13(2), 961–981, doi:10.5194/acp-13-961-2013, 2013.

DeCarlo, P. F., Slowik, J. G., Worsnop, D. R., Davidovits, P. and Jimenez, J. L.: Particle morphology and density characterization by combined mobility and aerodynamic diameter measurements. Part 1: Theory, Aerosol Sci. Technol., 38(12), 1185–1205, doi:10.1080/027868290903907, 2004.

El Haddad, I., D'Anna, B., Temime-Roussel, B., Nicolas, M., Boreave, A., Favez, O., Voisin, D., Sciare, J., George, C., Jaffrezo, J. L., Wortham, H. and Marchand, N.: Towards a better understanding of the origins, chemical composition and aging of oxygenated organic aerosols: Case study of a Mediterranean industrialized environment, Marseille, Atmos. Chem. Phys., 13(15), 7875–7894, doi:10.5194/acp-13-7875-2013, 2013.

He, L. Y., Lin, Y., Huang, X. F., Guo, S., Xue, L., Su, Q., Hu, M., Luan, S. J. and Zhang, Y. H.: Characterization of high-resolution aerosol mass spectra of primary organic aerosol emissions from Chinese cooking and biomass burning, Atmos. Chem. Phys., 10(23), 11535–11543, doi:10.5194/acp-10-11535-2010, 2010.

Massagué, J., Carnerero, C., Escudero, M., Baldasano, J. M., Alastuey, A. and Querol, X.: 2005–2017 ozone trends and potential benefits of local measures as deduced from air quality measurements in the north of the Barcelona Metropolitan Area, Atmos. Chem. Phys. Discuss., (2), 1–28, doi:10.5194/acp-2019-33, 2019.

Middlebrook, A. M., Bahreini, R., Jimenez, J. L. and Canagaratna, M. R.: Evaluation of composition-dependent collection efficiencies for the Aerodyne aerosol mass spectrometer using field data, Aerosol Sci. Technol., 46(3), 258–271, doi:10.1080/02786826.2011.620041, 2012.

Millán, M. M.: Extreme hydrometeorological events and climate change predictions in Europe, J. Hydrol., 518(PB), 206–224, doi:10.1016/j.jhydrol.2013.12.041, 2014.

Millán, M. M., Salvador, R., Mantilla, E. and Kallos, G.: Photooxidant dynamics in the Mediterranean basin in summer: Results from European research projects, J. Geophys. Res. Atmos., 102(7), 8811–8823, doi:10.1029/96jd03610, 1997.

Minguillón, M. C., Perron, N., Querol, X., Szidat, S., Fahrni, S. M., Alastuey, A., Jimenez, J. L., Mohr, C., Ortega, A. M., Day, D. A., Lanz, V. A., Wacker, L., Reche, C., Cusack, M., Amato, F., Kiss, G., Hoffer, A., Decesari, S., Moretti, F., Hillamo,

https://doi.org/10.5194/acp-2020-1244
Preprint. Discussion started: 16 December 2020




R., Teinilä, K., Seco, R., Peñuelas, J., Metzger, A., Schallhart, S., Müller, M., Hansel, A., Burkhart, J. F., Baltensperger, U. and Prévôt, A. S. H.: Fossil versus contemporary sources of fine elemental and organic carbonaceous particulate matter during the DAURE campaign in Northeast Spain, Atmos. Chem. Phys., 11(23), 12067–12084, doi:10.5194/acp-11-12067-2011, 2011.

Minguillón, M. C., Ripoll, A., Pérez, N., Prévôt, A. S. H., Canonaco, F., Querol, X. and Alastuey, A.: Chemical characterization of submicron regional background aerosols in the western Mediterranean using an Aerosol Chemical Speciation Monitor, Atmos. Chem. Phys., 15(11), 6379–6391, doi:10.5194/acp-15-6379-2015, 2015.

Minguillón, M. C., Pérez, N., Marchand, N., Bertrand, A., Temime-Roussel, B., Agrios, K., Szidat, S., van Drooge, B., Sylvestre, A., Alastuey, A., Reche, C., Ripoll, A., Marco, E., Grimalt, J. O. and Querol, X.: Secondary organic aerosol origin in an urban environment: influence of biogenic and fuel combustion precursors, Faraday Discuss., 189, 337–359, doi:10.1039/c5fd00182j, 2016.

Mohr, C., DeCarlo, P. F., Heringa, M. F., Chirico, R., Slowik, J. G., Richter, R., Reche, C., Alastuey, A., Querol, X., Seco, R., Peñuelas, J., Jiḿenez, J. L., Crippa, M., Zimmermann, R., Baltensperger, U. and Prév̂ot, A. S. H.: Identification and quantification of organic aerosol from cooking and other sources in Barcelona using aerosol mass spectrometer data, Atmos. Chem. Phys., 12(4), 1649–1665, doi:10.5194/acp-12-1649-2012, 2012.

Mohr, C., DeCarlo, P. F., Heringa, M. F., Chirico, R., Richter, R., Crippa, M., Querol, X., Baltensperger, U. and Prévôt, A. S. H.: Spatial Variation of Aerosol Chemical Composition and Organic Components Identified by Positive Matrix Factorization in the Barcelona Region, Environ. Sci. Technol., 49(17), 10421–10430, doi:10.1021/acs.est.5b02149, 2015.

Ng, N. L., Canagaratna, M. R., Zhang, Q., Jimenez, J. L., Tian, J., Ulbrich, I. M., Kroll, J. H., Docherty, K. S., Chhabra, P. S., Bahreini, R., Murphy, S. M., Seinfeld, J. H., Hildebrandt, L., Donahue, N. M., Decarlo, P. F., Lanz, V. A., Prévôt, A. S. H., Dinar, E., Rudich, Y. and Worsnop, D. R.: Organic aerosol components observed in Northern Hemispheric datasets from Aerosol Mass Spectrometry, Atmos. Chem. Phys., 10(10), 4625–4641, doi:10.5194/acp-10-4625-2010, 2010.

Ng, N. L., Herndon, S. C., Trimborn, A., Canagaratna, M. R., Croteau, P. L., Onasch, T. B., Sueper, D., Worsnop, D. R., Zhang, Q., Sun, Y. L. and Jayne, J. T.: An Aerosol Chemical Speciation Monitor (ACSM) for routine monitoring of the composition and mass concentrations of ambient aerosol, Aerosol Sci. Technol., 45(7), 770–784, doi:10.1080/02786826.2011.560211, 2011.

Paatero, P.: The Multilinear Engine—A Table-Driven, Least Squares Program for Solving Multilinear Problems, Including the n-Way Parallel Factor Analysis Model, J. Comput. Graph. Stat., 8(4), 854–888, doi:10.1080/10618600.1999.10474853, 1999.

Paatero, P. and Tapper, U.: Positive matrix factorization: A non-negative factor model with optimal utilization of error estimates of data values, Environmetrics, 5(2), 111–126, doi:10.1002/env.3170050203, 1994.

Pérez, C., Sicard, M., Jorba, O., Comerón, A. and Baldasano, J. M.: Summertime re-circulations of air pollutants over the north-eastern Iberian coast observed from systematic EARLINET lidar measurements in Barcelona, Atmos. Environ., 38(24), 3983–4000, doi:10.1016/j.atmosenv.2004.04.010, 2004.

Pey, J., Querol, X., Alastuey, A., Rodríguez, S., Putaud, J. P. and Van Dingenen, R.: Source apportionment of urban fine and ultra-fine particle number concentration in a Western Mediterranean city, Atmos. Environ., 43(29), 4407–4415, doi:10.1016/j.atmosenv.2009.05.024, 2009.

Pey, J., Pérez, N., Querol, X., Alastuey, A., Cusack, M. and Reche, C.: Intense winter atmospheric pollution episodes affecting the Western Mediterranean, Sci. Total Environ., 408(8), 1951–1959, doi:10.1016/j.scitotenv.2010.01.052, 2010.

Reche, C., Viana, M., Amato, F., Alastuey, A., Moreno, T., Hillamo, R., Teinilä, K., Saarnio, K., Seco, R., Peñuelas, J., Mohr, C., Prévôt, A. S. H. and Querol, X.: Biomass burning contributions to urban aerosols in a coastal Mediterranean City, Sci. Total Environ., 427–428, 175–190, doi:10.1016/j.scitotenv.2012.04.012, 2012.

Reyes-Villegas, E., Bannan, T., Le Breton, M., Mehra, A., Priestley, M., Percival, C., Coe, H. and Allan, J. D.: Online Chemical Characterization of Food-Cooking Organic Aerosols: Implications for Source Apportionment, Environ. Sci. Technol., 52(9), 5308–5318, doi:10.1021/acs.est.7b06278, 2018.

Ripoll, A., Pey, J., Minguillón, M. C., Pérez, N., Pandolfi, M., Querol, X. and Alastuey, A.: Three years of aerosol mass, black carbon and particle number concentrations at Montsec (southern Pyrenees, 1570 m a.s.l.), Atmos. Chem. Phys., 14(8), 4279–4295, doi:10.5194/acp-14-4279-2014, 2014.

Ripoll, A., Minguillón, M. C., Pey, J., Jimenez, J. L., Day, D. A., Sosedova, Y., Canonaco, F., Prévôt, A. S. H., Querol, X. and Alastuey, A.: Long-term real-time chemical characterization of submicron aerosols at Montsec (southern Pyrenees, 1570 m a.s.l.), Atmos. Chem. Phys., 15(6), 2935–2951, doi:10.5194/acp-15-2935-2015, 2015.

Saiz-Lopez, A., Borge, R., Notario, A., Adame, J. A., Paz, D. D. La, Querol, X., Artíñano, B., Gómez-Moreno, F. J. and Cuevas, C. A.: Unexpected increase in the oxidation capacity of the urban atmosphere of Madrid, Spain, Sci. Rep., 7, 1–11, doi:10.1038/srep45956, 2017.



Servei Meteorològic de Catalunya: Històric de mapes de precipitació mensual - Servei Meteorològic de Catalunya | Meteocat, Històric mapes precipitació [online] Available from: https://www.meteo.cat/wpweb/climatologia/el-clima-ahir/historic-cartografia-climatica/historic-de-mapes-de-precipitacio-mensual/ (Accessed 1 July 2020a), 2020.

Servei Meteorològic de Catalunya: Històric de mapes de temperatura mensual - Servei Meteorològic de Catalunya | Meteocat, Històric mapes Temp. [online] Available from: https://www.meteo.cat/wpweb/climatologia/el-clima-ahir/historic-cartografia-climatica/historic-de-mapes-de-temperatura-mensual/ (Accessed 16 June 2020b), 2020.

Shi, Y., Chen, J., Hu, D., Wang, L., Yang, X. and Wang, X.: Airborne submicron particulate (PM1) pollution in Shanghai, China: Chemical variability, formation/dissociation of associated semi-volatile components and the impacts on visibility, Sci. Total Environ., 473–474, 199–206, doi:10.1016/J.SCITOTENV.2013.12.024, 2014.

Shrivastava, M., Cappa, C. D., Fan, J., Goldstein, A. H., Guenther, A. B., Jimenez, J. L., Kuang, C., Laskin, A., Martin, S. T., Ng, N. L., Petaja, T., Pierce, J. R., Rasch, P. J., Roldin, P., Seinfeld, J. H., Shilling, J., Smith, J. N., Thornton, J. A., Volkamer, R., Wang, J., Worsnop, D. R., Zaveri, R. A., Zelenyuk, A. and Zhang, Q.: Recent advances in understanding secondary organic aerosol: Implications for global climate forcing, Rev. Geophys., 55(2), 509–559, doi:10.1002/2016RG000540, 2017.

Stein, A. F., Draxler, R. R., Rolph, G. D., Stunder, B. J. B., Cohen, M. D. and Ngan, F.: Noaa's hysplit atmospheric transport and dispersion modeling system, Bull. Am. Meteorol. Soc., 96(12), 2059–2077, doi:10.1175/BAMS-D-14-00110.1, 2015.

Tobler, A., Skiba, A., Wang, D., Croteau, P., Styszko, K., Nęcki, J., Baltensperger, U., Slowik, J. and Prévôt, A.: Improved chloride quantification in quadrupole aerosol chemical speciation monitors (Q-ACSMs), Atmos. Meas. Tech. Discuss., 36(May), 1–17, doi:10.5194/amt-2020-117, 2020.

Trippetta, S., Sabia, S. and Caggiano, R.: Fine aerosol particles (PM1): natural and anthropogenic contributions and health risk assessment, Air Qual. Atmos. Heal., 9(6), 621–629, doi:10.1007/s11869-015-0373-0, 2016.

WHO: Ambient air pollution: A global assessment of exposure and burden of disease, 2016.

WHO: Ambient (outdoor) air pollution, [online] Available from: https://www.who.int/news-room/fact-sheets/detail/ambient-(outdoor)-air-quality-and-health (Accessed 23 July 2020), 2018.

Xu, W., Lambe, A., Silva, P., Hu, W., Onasch, T., Williams, L., Croteau, P., Zhang, X., Renbaum-Wolff, L., Fortner, E., Jimenez, J. L., Jayne, J., Worsnop, D. and Canagaratna, M.: Laboratory evaluation of species-dependent relative ionization efficiencies in the Aerodyne Aerosol Mass Spectrometer, Aerosol Sci. Technol., 52(6), 626–641, doi:10.1080/02786826.2018.1439570, 2018.

Yang, B. Y., Guo, Y., Morawska, L., Bloom, M. S., Markevych, I., Heinrich, J., Dharmage, S. C., Knibbs, L. D., Lin, S., Yim, S. H. L., Chen, G., Li, S., Zeng, X. W., Liu, K. K., Hu, L. W. and Dong, G. H.: Ambient PM1 air pollution and cardiovascular disease prevalence: Insights from the 33 Communities Chinese Health Study, Environ. Int., 123(December 2018), 310–317, doi:10.1016/j.envint.2018.12.012, 2019.

Yang, M., Chu, C., Bloom, M. S., Li, S., Chen, G., Heinrich, J., Markevych, I., Knibbs, L. D., Bowatte, G., Dharmage, S. C., Komppula, M., Leskinen, A., Hirvonen, M. R., Roponen, M., Jalava, P., Wang, S. Q., Lin, S., Zeng, X. W., Hu, L. W., Liu, K. K., Yang, B. Y., Chen, W., Guo, Y. and Dong, G. H.: Is smaller worse? New insights about associations of PM 1 and respiratory health in children and adolescents, Environ. Int., 120(August), 516–524, doi:10.1016/j.envint.2018.08.027, 2018.

Zhang, Q., Jimenez, J. L., Canagaratna, M. R., Allan, J. D., Coe, H., Ulbrich, I., Alfarra, M. R., Takami, A., Middlebrook, A. M., Sun, Y. L., Dzepina, K., Dunlea, E., Docherty, K., DeCarlo, P. F., Salcedo, D., Onasch, T., Jayne, J. T., Miyoshi, T., Shimono, A., Hatakeyama, S., Takegawa, N., Kondo, Y., Schneider, J., Drewnick, F., Borrmann, S., Weimer, S., Demerjian, K., Williams, P., Bower, K., Bahreini, R., Cottrell, L., Griffin, R. J., Rautiainen, J., Sun, J. Y., Zhang, Y. M. and Worsnop, D. R.: Ubiquity and dominance of oxygenated species in organic aerosols in anthropogenically-influenced Northern Hemisphere midlatitudes, Geophys. Res. Lett., 34(13), 1–6, doi:10.1029/2007GL029979, 2007.

Zhang, Y., Favez, O., Petit, J. E., Canonaco, F., Truong, F., Bonnaire, N., Crenn, V., Amodeo, T., Prévôt, A. S. H., Sciare, J., Gros, V. and Albinet, A.: Six-year source apportionment of submicron organic aerosols from near-continuous highly time-resolved measurements at SIRTA (Paris area, France), Atmos. Chem. Phys., 19(23), 14755–14776, doi:10.5194/acp-19-14755-2019, 2019a.

Zhang, Y., Favez, O., Petit, J. E., Canonaco, F., Truong, F., Bonnaire, N., Crenn, V., Amodeo, T., Prévôt, A. S. H., Sciare, J., Gros, V. and Albinet, A.: Six-year source apportionment of submicron organic aerosols from near-continuous highly time-resolved measurements at SIRTA (Paris area, France), Atmos. Chem. Phys., 19(23), 14755–14776, doi:10.5194/acp-19-14755-2019, 2019b.

https://doi.org/10.5194/acp-2020-1244
Preprint. Discussion started: 16 December 2020


Atmospheric Chemistry and Physics Discussions

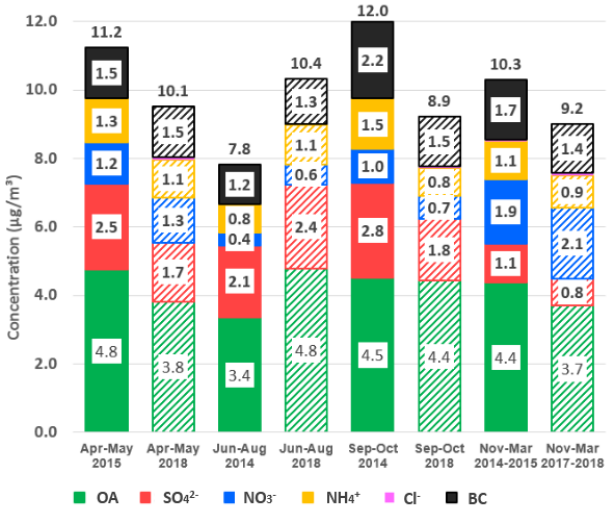


**Figure 1. Seasonal bar plot of ACSM species and BC mean concentrations for periods A, with solid bars and B, with weft bars.**

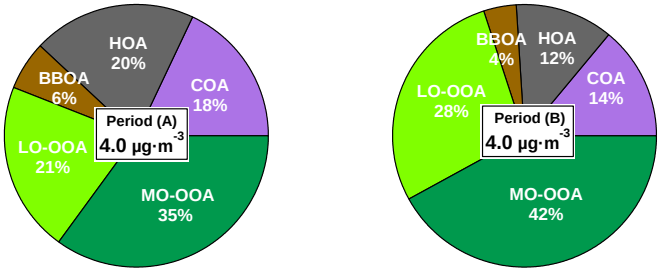


**Figure 2. Average OA source apportionment for periods A and B and concentrations of apportioned OA for period A and period B.**

https://doi.org/10.5194/acp-2020-1244
Preprint. Discussion started: 16 December 2020


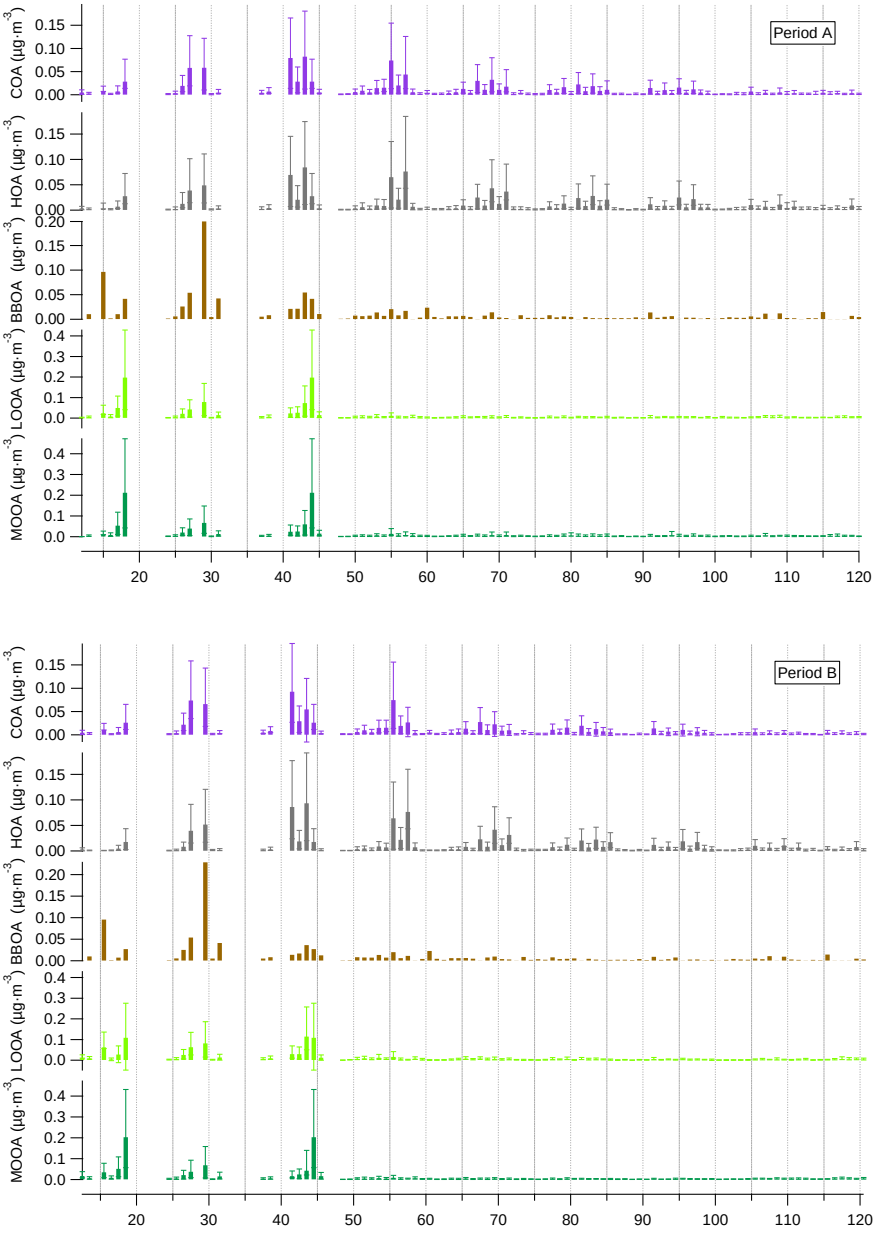


560

**Figure 3. Mass spectra of the five OA factors for periods A and B. Stick lines are averaged values over all seasons for a given period. Error bars represent maximum and minimum values for the seasonal analysis.**

https://doi.org/10.5194/acp-2020-1244
Preprint. Discussion started: 16 December 2020


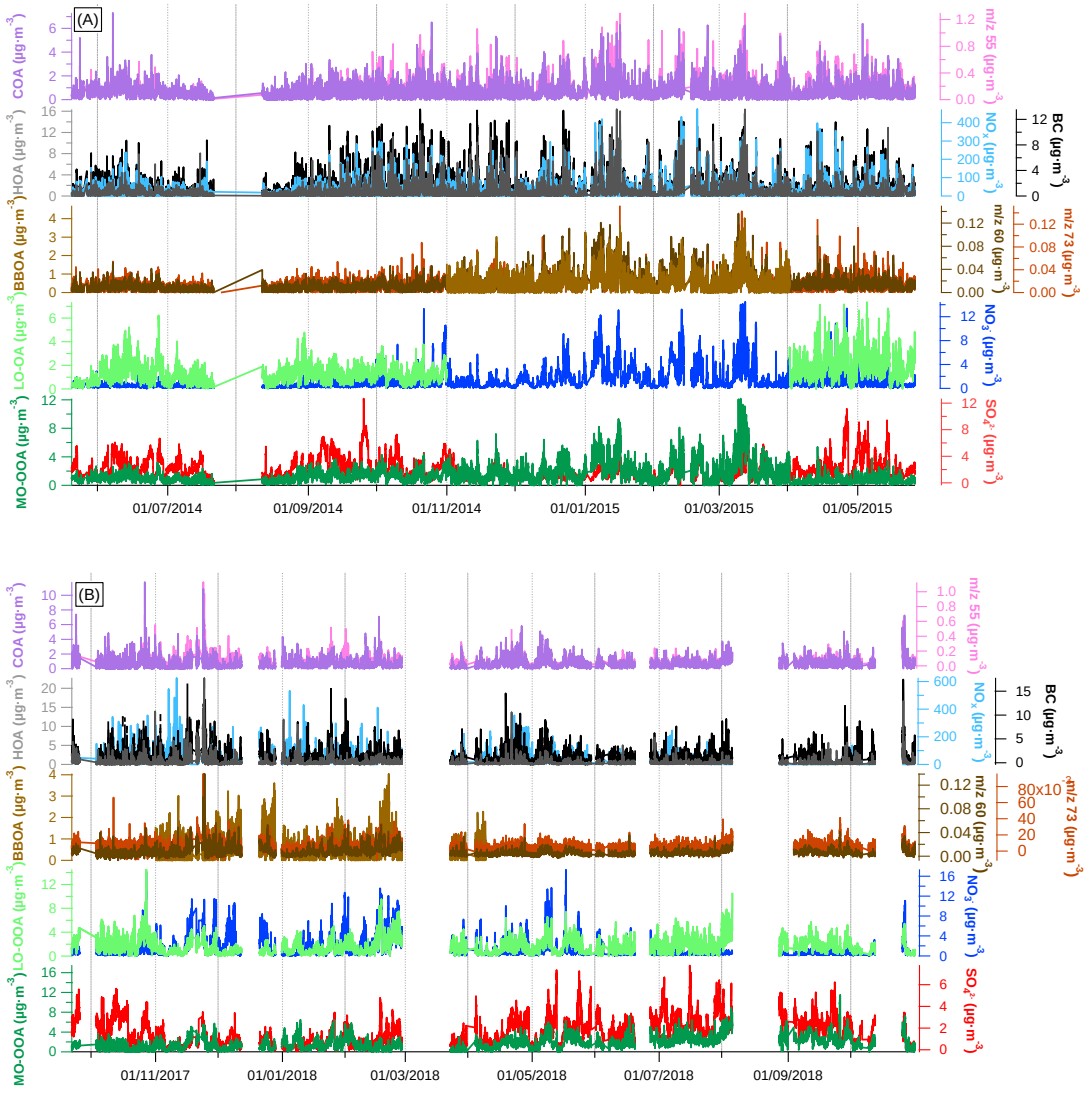


565 **Figure 4. Time series of identified OA sources (left axis) and their markers (right axis) in period A (top) and period B (bottom).**

https://doi.org/10.5194/acp-2020-1244
Preprint. Discussion started: 16 December 2020


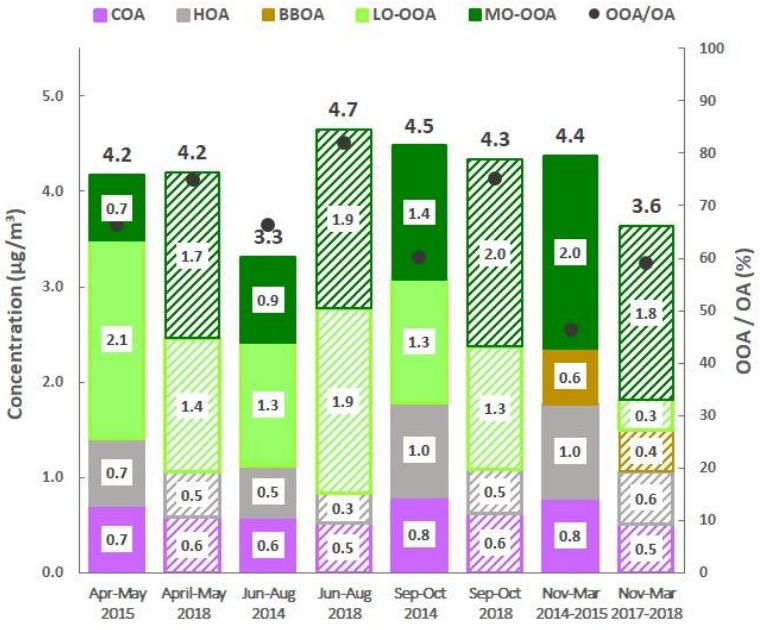


**Figure 5. Seasonal OA source apportionment, with solid and weft stacked bars respectively for period A and B and OA concentrations at top. Markers show the oxygenated organic aerosol proportion with respect to total OA.**

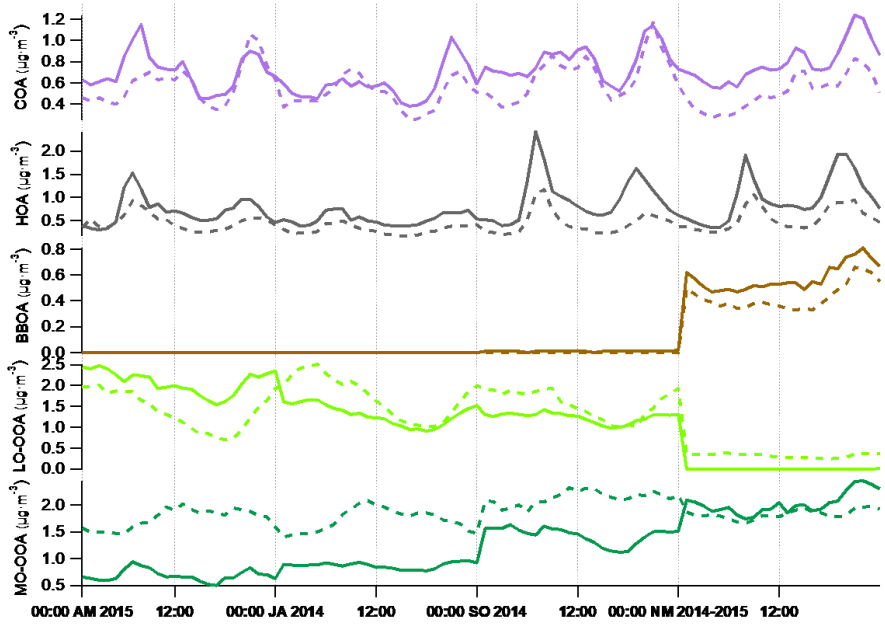


570

**Figure 6. Diel cycle sorted by seasons for the five OA factors for period A (solid lines) and B (dashed lines).**

https://doi.org/10.5194/acp-2020-1244
Preprint. Discussion started: 16 December 2020


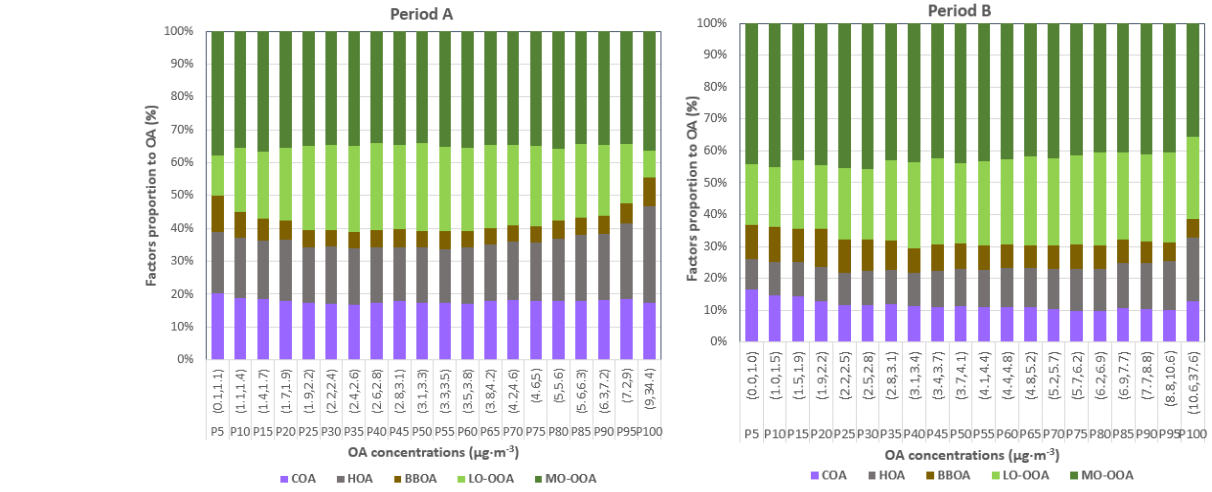


**Figure 7. Proportion of organic sources concentrations relative to OA concentrations as a function of OA. Ranges in the x-axis correspond to the numerical values of the percentiles in steps of 5.**

575

**(a)**

580

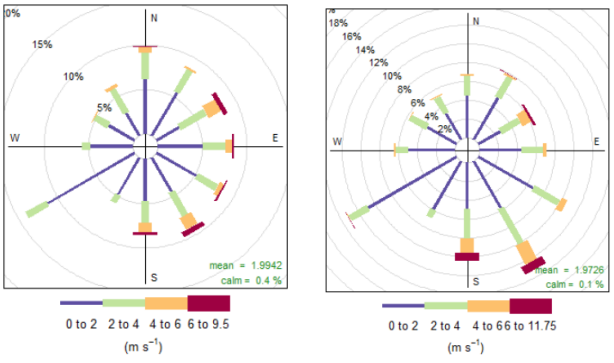


**(b)**

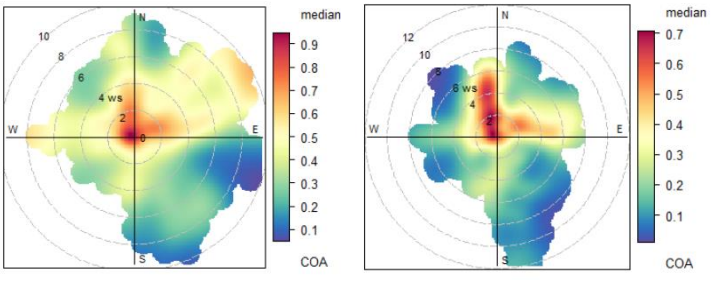

https://doi.org/10.5194/acp-2020-1244
Preprint. Discussion started: 16 December 2020


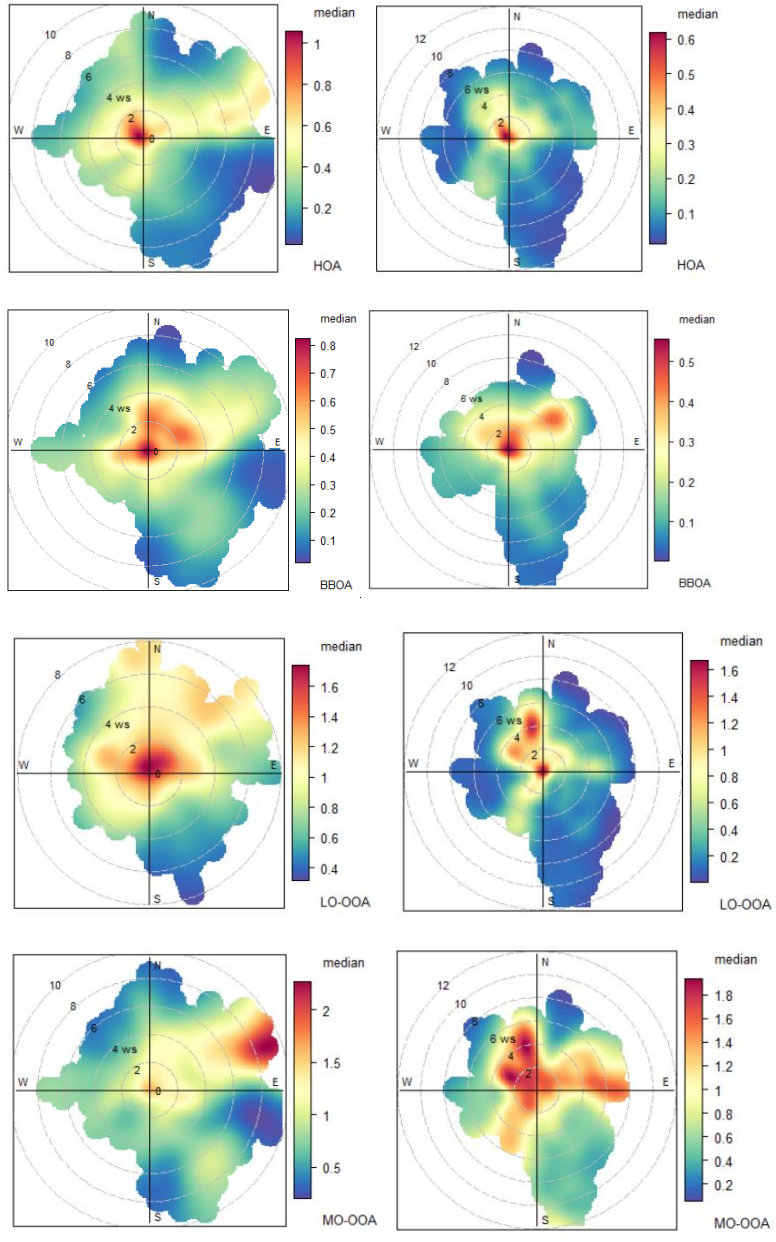


**Figure 8. Wind dependence of OA factors. (a) Windrose plots showing frequency of counts regarding wind direction and wind speed (m/s). (b) Polar plots color-coded by median mass concentrations (μg/m$^3$). In both cases, plots are arranged to the left for Period A and to the right for Period B.**

https://doi.org/10.5194/acp-2020-1244
Preprint. Discussion started: 16 December 2020


Atmospheric Chemistry and Physics Discussions

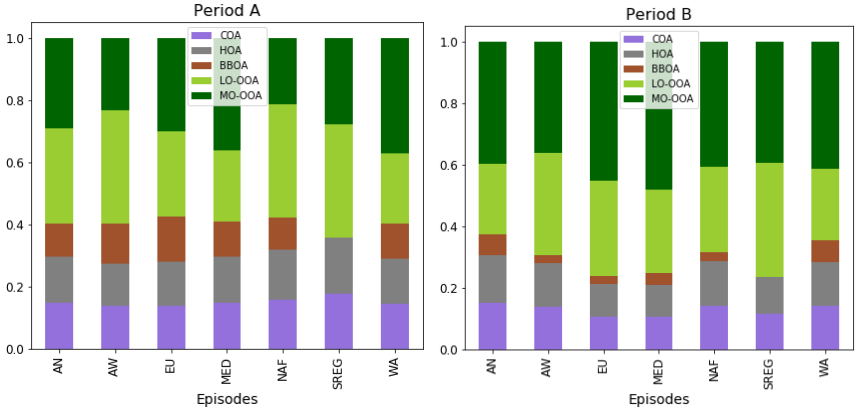


**Figure 9. Bar chart of factor proportion to total concentrations per each factor grouped by episodes for period A and B.**

595